

Anhydrite precipitation and the extent of hydrothermal recharge zones at ocean ridge crests

Robert P. Lowell and Yufeng Yao

School of Earth and Atmospheric Sciences, Georgia Institute of Technology, Atlanta, Georgia, USA

Received 21 September 2001; revised 20 February 2002; accepted 25 February 2002; published 13 September 2002.

[1] We develop mathematical models to investigate anhydrite precipitation in hydrothermal recharge zones at ocean ridge axes. We first consider constant flow during hydrothermal recharge to estimate the depth, the depth interval over which anhydrite precipitation would occur, and the initial rate of porosity reduction. We find that the smaller the downward mass flux, the shallower and more broadly distributed the region of precipitation. For values of downward mass flux similar to that for high-temperature black smoker systems, the porosity would be clogged significantly in a matter of months to years depending upon the initial porosity. We then consider anhydrite precipitation in a buoyancy-driven single-pass model in which the reduction in permeability resulting from anhydrite precipitation exerts a feedback on the flow rate. This model gives results similar to the constant flow model for the initial depth, depth interval, and rate of porosity reduction. The effect of the permeability clogging on the flow rate, however, is twofold. First, the zone of anhydrite precipitation shallows and broadens as the flow rate decreases, thus allowing deeply deposited anhydrite to be preserved temporarily. Second, if the recharge area of the same size as the discharge area, anhydrite precipitation rapidly reduces the flow rate and the heat output of the hydrothermal system. If the initial porosity of the recharge zone is 1%, the area of the recharge zone must be ~ 10 – 100 times that of the discharge zone to maintain near steady state conditions for time periods of decades to hundreds of years. This result implies that recharge zones may be quite large and extend off axis as well as along axis. *INDEX TERMS*: 3015 Marine Geology and Geophysics: Heat flow (benthic) and hydrothermal processes; 8135 Tectonophysics: Hydrothermal systems (8424); 3035 Marine Geology and Geophysics: Midocean ridge processes; 4832 Oceanography: Biological and Chemical: Hydrothermal systems; *KEYWORDS*: hydrothermal systems, anhydrite, mid-ocean ridges, permeability

Citation: Lowell, R. P., and Y. Yao, Anhydrite precipitation and the extent of hydrothermal recharge zones at ocean ridge crests, *J. Geophys. Res.*, 107(B9), 2183, doi:10.1029/2001JB001289, 2002.

1. Introduction

[2] The discovery of seafloor hydrothermal systems more than two decades ago has revolutionized the understanding of thermal, geochemical, and biological processes on Earth. Seafloor hydrothermal systems transport nearly 33% of the global oceanic heat flux [Williams and Von Herzen, 1974; Sclater *et al.*, 1980; Stein and Stein, 1994]. Chemical reactions between hydrothermal seawater and basaltic crustal rocks result in chemical exchanges that impact the global geochemical cycles of the lithosphere and the oceans [Wolery and Sleep, 1976; Edmond *et al.*, 1979; Thompson, 1983]. Hydrothermal fluids serve as an energy resource for complex chemosynthetic biological ecosystems [Jannasch and Wirsén, 1979; Jannasch, 1983, 1995; Shank *et al.*, 1998]. Much of the hydrothermal heat transfer and geochemical cycling occurs at relatively low-temperature away from the ridge axis [e.g., Elderfield and Schultz, 1996]. At ridge axes, however, heat transfer from subsurface magma and heated crustal rocks

results in water-rock reactions at temperatures of $\sim 400^\circ\text{C}$; the altered, mineral-laden fluids then emerge at the seafloor as black smoker vents.

[3] Although considerable data exist on the heat flux, temperature, and chemistry of the vent fluids [e.g., Von Damm, 1995], relatively little is known of the recharge zones. Though some conceptual models of ridge-crest hydrothermal activity propose that deep recharge occurs primarily along axis [Haymon *et al.*, 1991], it is generally thought that the recharge zones are more extensive than discharge zones and that deep recharge may be fully three-dimensional. Recharge zones are difficult to detect, particularly in bare rock environments at ridge crests. Johnson and Hutnak [1997] have developed a method for measuring heat flow on sediment-free oceanic crust and have detected an area of low heat flow that may represent hydrothermal recharge into pillow basalts. Becker *et al.* [1996] have detected local areas of low heat flow on the TAG hydrothermal mound that also suggests seawater recharge. Such data are sparse at present, however.

[4] Another issue concerning recharge at high temperature systems concerns the fate of seawater sulfate. Sea-

water contains ~ 10 mmol kg^{-1} concentration of Ca^{2+} and 28 mmol kg^{-1} of SO_4^{2-} , and laboratory experiments have shown that upon heating to $\sim 150^\circ\text{C}$, anhydrite (CaSO_4) will precipitate from seawater [Blount and Dickson, 1969; Bischoff and Seyfried, 1978]. Up to $\sim 250^\circ\text{C}$, Ca^{2+} and SO_4^{2-} are lost in equal amounts, and therefore a significant amount of SO_4^{2-} remains after the Ca^{2+} is removed from seawater [Bischoff and Seyfried, 1978]. When seawater reacts with basalt, however, laboratory experiments show that anhydrite precipitates initially from seawater, but as the temperature becomes $>150^\circ\text{C}$ additional Ca^{2+} is exchanged for Mg^{2+} in seawater, thus permitting the formation of more anhydrite than would precipitate from just heating seawater [Bischoff and Dickson, 1975; Seyfried and Bischoff, 1981; Mottl, 1983]. It is thought some seawater sulfate enters the high-temperature reaction zone where it is reduced to sulfide [e.g., Shanks et al., 1981; Alt et al., 1989]. Sulfate is essentially absent in high-temperature vent fluids and the sulfur in vent fluids occurring as H_2S carries a magmatic isotopic signature, supporting the idea that a considerable fraction of seawater sulfate is removed from the circulation system [Von Damm et al., 1985; Bowers et al., 1988; Alt et al., 1989]. The isotopic signature of anhydrite found in fractures in sheeted dikes sampled by drilling at Deep Sea Drilling Project/Ocean Drilling Program (DSDP/ODP) site 504B is consistent with its formation upon heating of seawater during recharge [McDuff and Edmond, 1982; Alt et al., 1989]. There is much less anhydrite present in the oceanic crust than would be expected from anhydrite precipitation [Alt et al., 1989; Teagle et al., 1998]. This occurs in part because of the retrograde solubility of anhydrite below 150°C [Mottl et al., 1979]. Thus, as the crust moves off axis, the anhydrite dissolves and reenters the water column or other mineral phases [Alt et al., 1986, 1989].

[5] The issues of recharge area and anhydrite precipitation upon heating of seawater during recharge become particularly important in models of high-temperature ridge crest hydrothermal circulation. Then precipitation of anhydrite during recharge could reduce porosity and permeability and thus affect the fluid flow rate and thermal characteristics of a high-temperature system. Mottl [1983] estimated that a hundred meter thick crustal layer in a 25 km^2 recharge zone with initially 20% porosity would be sealed by anhydrite precipitation in 10^4 years. Sleep [1991] developed a steady state mathematical model of anhydrite precipitation at a ridge axis to determine scenarios in which precipitated anhydrite would be preserved at depth in the crust. He further suggested that anhydrite precipitation could clog throughgoing fractures in the recharge zone but that areas of widespread porous discharge would not be clogged. Recently, Fontaine et al. [2001] considered anhydrite precipitation during porous medium convection in a slot. Their results focused on anhydrite precipitation during mixing of hot upwelling fluids with cold seawater and did not address the problem of anhydrite precipitation upon direct heating of downward flowing seawater. Both Mottl [1983] and Sleep [1991] addressed large-scale circulation rather than the smaller ~ 1 km scale appropriate for an individual system high-temperature system.

[6] In this paper we address the reduction of porosity and permeability in a ridge-crest recharge zone resulting from

anhydrite precipitation using a single-pass model to investigate a ridge-axis black smoker system. We place the broad conclusions of Mottl [1983] and Sleep [1991] on a more quantitative foundation. We do not address details concerning the exact sites, environments, or mechanisms of formation of hydrothermal recharge. Rather we use the constraints provided by observed hydrothermal heat output, the principle of conservation of fluid mass, and calculated rates of porosity and permeability reduction as a result of anhydrite precipitation to provide insight into the size of hydrothermal recharge zones. The fact that hydrothermal heat losses occur globally to a lithospheric age of ~ 65 Ma [Stein and Stein, 1994] and the occurrence of vigorous hydrothermal discharge in young sediment-free lithosphere near ocean ridge crests indicates that seawater has relatively easy access to and egress from the lithosphere. In the following sections we develop the mathematical model and display the results. The results show that high-temperature recharge zones would be rapidly sealed as a result of anhydrite precipitation unless recharge occurs over a wide area. This suggests that hydrothermal recharge at ridge axes occurs from off axis as well as from along axis.

2. Mathematical Model

[7] To simulate anhydrite precipitation and its effect on the permeability of the hydrothermal recharge zone, we will apply the single-pass model [e.g., Lowell and Burnell, 1991; Lowell and Germanovich, 1994, 1997]. As shown schematically in Figure 1, cold seawater enters the recharge zone, penetrates to near the top of the magma lens at a depth $H \sim 1$ km, is heated, enters the discharge zone, and flows out at the surface. For simplicity, in this paper, we will not consider the detailed nature of heat transfer from the magma lens nor possible complications resulting from two-phase flow or brine formation. Rather an isothermal condition of $T = 350^\circ\text{C}$ will be used at the lower boundary.

[8] We will simulate anhydrite precipitation in the recharge zone using two different scenarios. First, we will consider steady state heat transfer with a constant downward fluid flow rate. In this case, anhydrite precipitation occurs upon heating because the solubility of anhydrite decreases with increasing temperature. The rate at which the porosity decreases then depends upon the flow rate, the thermal gradient with depth, and the slope of the anhydrite solubility curve. In this scenario, we will neglect the feedback between the reduction of porosity (and permeability) and the flow rate. This simple approach will be used to characterize the initial rate of porosity decrease and to show how the various model parameters affect the location of anhydrite precipitation and the rate of porosity reduction. Second, we will consider the full single-pass model driven by fluid buoyancy. Then the decrease in porosity will be calculated as in the first scenario but now porosity will be related to permeability through a power law relationship. Because the permeability is now a function of time, the fluid flow rate and the temperature are also functions of time. The distribution of anhydrite will then respond to the changes in thermal structure of the recharge zone. In this scenario we will not only investigate the changes in porosity but also the permeability, heat output, and location of anhydrite precipitation within the recharge zone. The goals of these calculations are

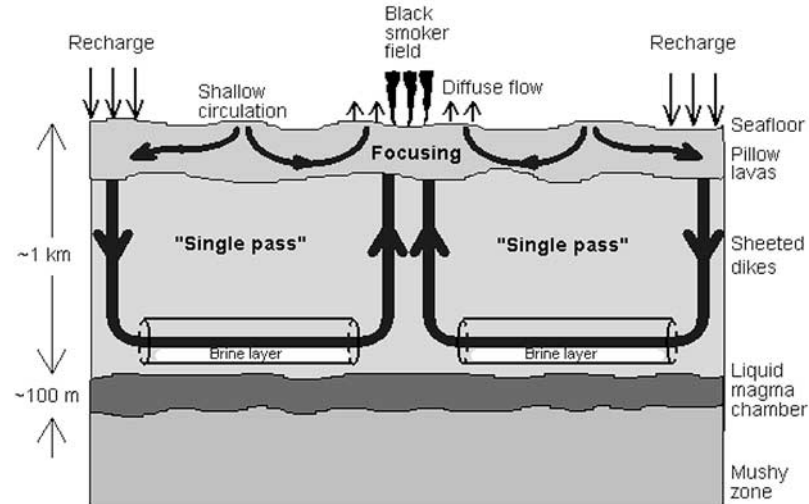


Figure 1. Cartoon of a single-pass model for hydrothermal circulation at a mid-ocean ridge crest [from Lowell and Germanovich, 1997].

to determine the rate at which anhydrite can seal permeability in a high-temperature hydrothermal recharge zone and discover whether this process can provide any constraints on the nature of the recharge zone itself.

[9] In each of these scenarios we assume the change in porosity ϕ as a function of time is expressed through a simple mass balance expression relating the change in pore volume to the rate at which concentration of anhydrite C in the fluid changes along the flow direction z [e.g., Wood and Hewett, 1982; Phillips, 1991; Lowell et al., 1993; Martin and Lowell, 2000]. That is,

$$\rho_{an} \frac{d(\phi/\phi_0)}{dt} = \frac{\rho_f u}{\phi_0} \frac{dC(P, T)}{dz}, \quad (1)$$

where ρ_{an} and ρ_f are the densities of the precipitating mineral and fluid, respectively, u is the Darcian velocity, and P is the pressure. The initial porosity, ϕ_0 , is inserted for later convenience. Parameters and their values are listed in Table 1. Equation (1) assumes that dispersion can be neglected relative to advection and that anhydrite precipitation can be written as a “gradient reaction,” in which the rate of precipitation is governed by the mineral solubility as the fluid moves along temperature and pressure gradients [Phillips, 1991]. This assumption implies that $C(P, T) = C_{eq}(P, T)$ (the equilibrium concentration), which is reasonable for the flow rates considered here. This assumption will be addressed further in section 4. Laboratory experiments also show that the pressure dependence of anhydrite solubility is considerable less than its temperature dependence for the range of pressure and temperature considered here [Blount and Dickson, 1969]. Upon neglecting the pressure term and employing the chain rule of differentiation, equation (1) becomes

$$\rho_{an} \frac{d(\phi/\phi_0)}{dt} = \frac{\rho_f u}{\phi_0} \frac{dC_{eq}(T)}{dT} \frac{dT}{dz}. \quad (2)$$

For the calculations below, the solubility of anhydrite in seawater is taken from the experimental results of Bischoff

and Seyfried [1978] for Pointe Huene seawater at $P = 500$ bars. Their data given at increments of 50°C between 150°C and 350°C are fit by a smooth curve as shown in Figure 2a. The smoothed derivative dC_{eq}/dT , as determined from their data averaged over 50°C intervals between 150°C and 350°C , is plotted in Figure 2b. Figure 2b shows that the

Table 1. Parameters and Values

Parameter	Definition	Value
A_r, A_d	area of recharge and discharge zones, respectively	
b	fracture spacing	
c	specific heat of rock	$10^3 \text{ J kg}^{-1} \text{ }^\circ\text{C}^{-1}$
c_f	specific heat of fluid	$4 \times 10^3 \text{ J kg}^{-1} \text{ }^\circ\text{C}^{-1}$
C	concentration of anhydrite in fluid	
C_{eq}	equilibrium concentration of anhydrite in fluid	
D	fracture width	
G	gravitational acceleration	9.8 m s^{-2}
H	depth of hydrothermal system	10^3 m
\hat{H}	buoyancy pressure head driving flow	
K	permeability	
L	length of flow path	
Pe	Peclet number	
P	pressure	
$\dot{P}(t)$	power output of hydrothermal system	
Q	mass flow rate per unit area	
\dot{Q}	total mass flow rate	
R	flow resistance	
t	time	
T	temperature	
T_0	temperature at base of hydrothermal system	350°C
U	Darcian velocity (specific discharge)	
Z	vertical Cartesian coordinate	
α_f	thermal expansion coefficient of fluid	$10^{-4} \text{ }^\circ\text{C}^{-1}$
ϕ_0	initial porosity	0.01 or 0.1
ϕ	porosity	
λ	thermal conductivity	$2.5 \text{ W m}^{-1} \text{ }^\circ\text{C}^{-1}$
ν	kinematic viscosity of fluid	
ρ	density of rock	$3 \times 10^3 \text{ kg m}^{-3}$
ρ_f	density of fluid	10^3 kg m^{-3}
ρ_{an}	density of anhydrite	$3 \times 10^3 \text{ kg m}^{-3}$
τ	sealing time	

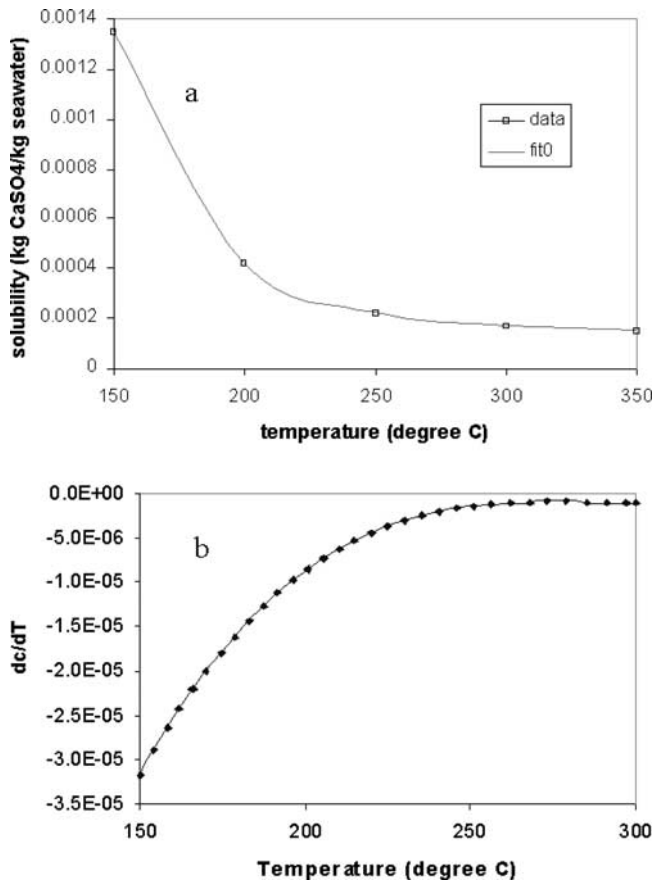


Figure 2. (a) Solubility of anhydrite as a function of temperature determined from *Bischoff and Seyfried* [1978]. (b) The derivative of the solubility as a function of temperature derived from the fit to the data of *Bischoff and Seyfried* [1978].

highest rate of decrease in solubility occurs between 150°C and 200°C. The rate of decrease in this interval is more than 40 times greater than that in the interval between 300°C and 350°C. To calculate the decrease in porosity as a function of time, equation (2) must be integrated, subject to knowing the Darcian velocity and the temperature gradient.

3. Results

3.1. Constant Flow Rate

[10] The easiest way to consider anhydrite precipitation during recharge is to assume a uniform Darcian flow rate u and to determine the resulting steady state temperature distribution. In this model (Figure 3), fluid enters the recharge zone at $z = 0$ at temperature $T = 0$ and exits at $z = H$ at $T = T_0$. The medium is assumed to have a constant initial porosity ϕ_0 .

[11] The steady state temperature distribution is determined from

$$\rho_f c_f u \frac{dT}{dz} = \lambda \frac{d^2 T}{dz^2}, \quad (3)$$

where c_f is the specific heat of fluid, and λ is the effective thermal conductivity of the rock-fluid mixture, respectively.

Then, the solution to equation (3) is

$$T = T_0 \frac{[1 - \exp(p_e z/H)]}{1 - \exp(p_e)}, \quad (4)$$

where $p_e = \rho_f c_f u H / \lambda$ is the Peclet number.

[12] Figure 4 shows temperature as a function of depth for $T_0 = 350^\circ\text{C}$, $H = 1$ km, and for a number of values of u . Values of u can be derived using observed heat flux at hydrothermal vents and estimates of the area of recharge zones. More details are provided by *Yao* [2001]. The range of values of u shown in Figure 4 encompasses most of the range of expected values, which according to *Yao* [2001] is $10^{-9} \text{ m s}^{-1} \leq u \leq 5 \times 10^{-4} \text{ m s}^{-1}$. The principal features to be taken from Figure 4 are that the higher the flow rate, the deeper the 150°C isotherm and the thinner the zone of anhydrite precipitation between 150°C and 350°C. That is, the greater the flow rate, the thinner and deeper the zone in which precipitation occurs. Figure 4 shows that when the $u = 10^{-7} \text{ m s}^{-1}$, anhydrite precipitation occurs below 620 m, whereas when velocity is 10^{-5} m s^{-1} , precipitation is concentrated below the 995 m depth.

[13] The initial rate of porosity decrease can be calculated from equation (2) using the temperature gradient found by taking the derivative of equation (4). This derivative is

$$\frac{dT}{dz} = \frac{T_0 p_e \exp(p_e z/H)}{H \exp(p_e) - 1}. \quad (5)$$

Upon substituting equation (5) into equation (2) and integrating one obtains

$$\frac{\phi - \phi_0}{\phi_0} = \left\{ \frac{\partial C_{eq}}{\partial T} \frac{\exp(p_e z/H)}{[\exp(p_e) - 1]} \left[\frac{T_0 c_f}{\lambda \rho_{an} \phi_0} \right] q^2 \right\} t, \quad (6)$$

where $q = \rho_f u$ is the mass flux per unit area. The inverse of the term in braces can be viewed as an approximate sealing

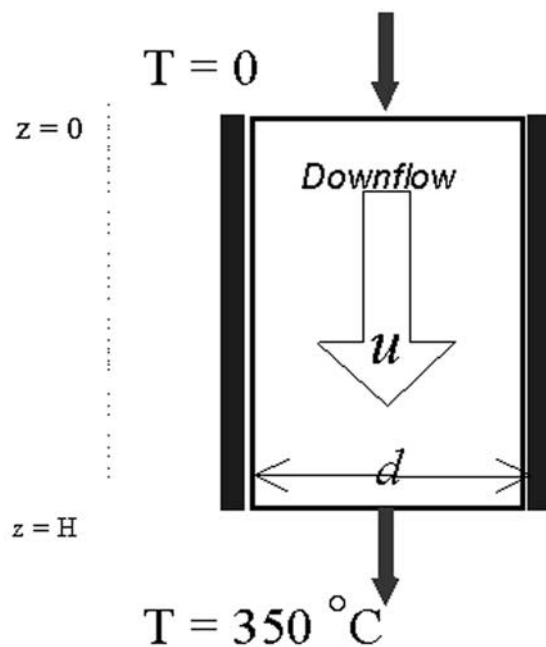


Figure 3. One-dimensional model for the recharge zone.

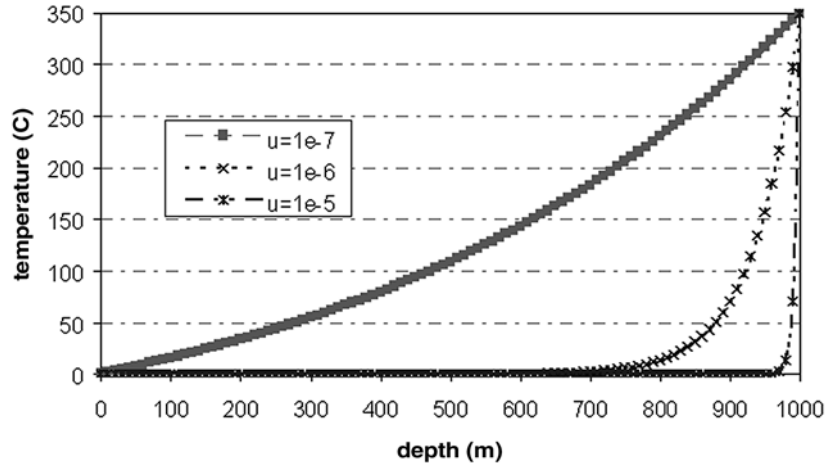


Figure 4. Steady state one-dimensional temperature distribution in the recharge zone for different Darcian flow rates.

time τ , provided the mass flux remains constant. The time τ is proportional to ϕ_0 and inversely proportional to q^2 . For large values of p_e , which is the case for the flow rates considered here, the first term in brackets obtains a maximum value of unity at $z = H$. The derivative of solubility is a maximum at 150°C, however. As a result, the initial rate of porosity decrease occurs near the 150°C isotherm for slower flow rates considered. At larger flow rates the region of porosity decrease is highly compressed, and the high rate of porosity decrease is dominated by the flow rate term in equation (6). The porosity distribution as a function depth at selected times for values of q are plotted in Figure 5, for an initial porosity $\phi_0 = 1\%$. If the initial porosity were higher (e.g., $\phi_0 = 10\%$), the shape of the curves would not change, but the times would be 10 times greater as indicated in equation (6).

[14] Figure 5 shows that the rate of porosity decrease is very rapid at higher flow rates ($q = 10^{-2} \text{ kg m}^{-2} \text{ s}^{-1}$), suggesting that anhydrite precipitation would rapidly seal the hydrothermal recharge zone. At low flow rates ($q = 10^{-4} \text{ kg m}^{-2} \text{ s}^{-1}$), appreciable sealing does not occur for hundreds of years. Because the total mass flow rate in black smoker systems is $\sim 100 \text{ kg s}^{-1}$, the mass flow rate per unit area used in Figure 5 corresponds to recharge areas of $10^4 \text{ m}^2 \leq A_r \leq 10^6 \text{ m}^2$. This relatively simple calculation suggests then that recharge areas must be considerably larger than discharge areas in order to prevent sealing rapid of recharge zones as a result of anhydrite precipitation.

[15] Treating anhydrite precipitation in the above manner involves a number of simplifying assumptions. Most importantly, we have assumed that the flow rate does not change even though the porosity of the medium varies with time. This leads to a lower bound estimate of the sealing time because as the flow rate decreases with decreasing porosity (and permeability), the rate of anhydrite precipitation would decrease. On the other hand, however, we have assumed there is no reaction between basalt and seawater. The result of such reactions would be to release Ca^{2+} from the rock in exchange for Mg^{2+} [Bischoff and Dickson, 1975; Seyfried and Bischoff, 1981; Mottl, 1983]; the additional Ca^{2+} could combine with the remaining SO_4^{2-} in seawater and lead to the precipitation of additional anhydrite. This process would lead to a greater

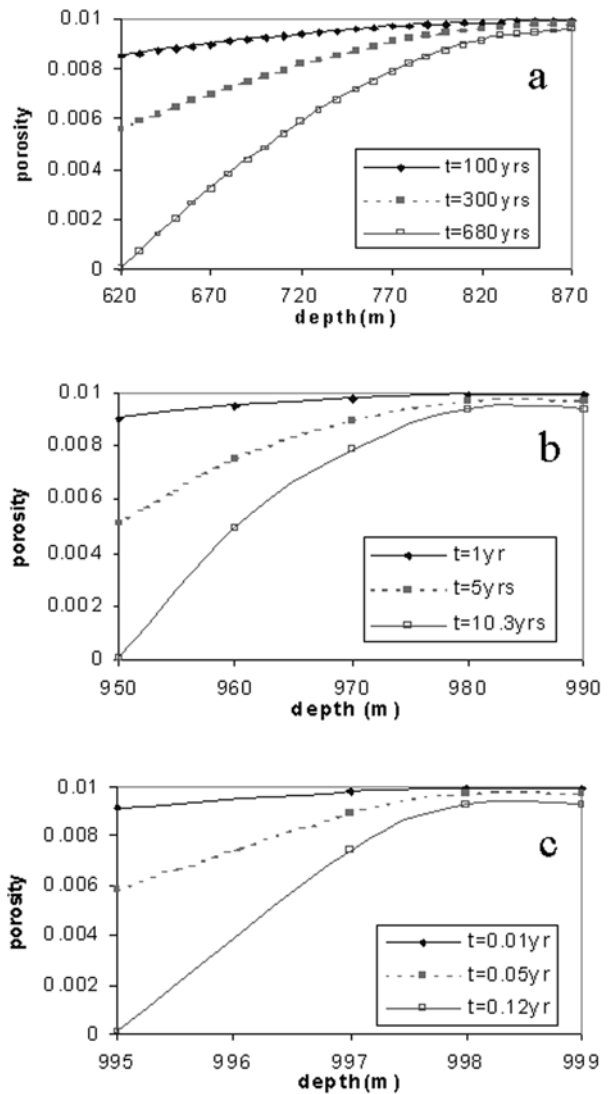


Figure 5. Porosity as a function of depth at selected times. Initial porosity = 1%. (a) $q = 10^{-4} \text{ kg m}^{-2} \text{ s}^{-1}$, (b) $q = 10^{-3} \text{ kg m}^{-2} \text{ s}^{-1}$, (c) $q = 10^{-2} \text{ kg m}^{-2} \text{ s}^{-1}$, respectively.

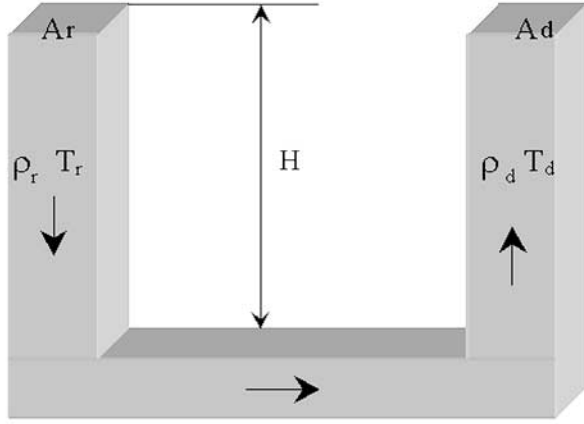


Figure 6. A schematic of the full single-pass model shown in Figure 1 used for calculations of anhydrite precipitation.

rate of anhydrite precipitation than considered above. We have also neglected the effect of other precipitates that may arise upon heating of seawater, such as magnesium oxysulfate [Bischoff and Seyfried, 1978] or that may result from low-temperature water-rock reactions. In section 3.2 we consider anhydrite precipitation in the context of the full buoyancy-driven single-pass model of Figure 1. This enables a treatment of the feedback of anhydrite precipitation on the flow rate. Thus both dT/dz and q become functions of time. We also allow the viscosity to be a function of time, but we still neglect the addition of Ca^{2+} as a result of basalt-seawater reaction at high temperature.

3.2. Variable Flow Rate: The Full Single-Pass Model

[16] Although the result for constant flow rate is instructive, it is important to investigate the feedback resulting from porosity and permeability changes to the system by using a full single-pass model. When considering the full single-pass model, the fluid flow is driven by buoyancy differences between the recharge and discharge zones [e.g., Lowell, 1975, 1991; Elder, 1981; Pascoe and Cann, 1995; Germanovich et al., 2001]. Then, as porosity and permeability are reduced as a result of anhydrite precipitation, the flow rate will decrease. This in turn will affect the temperature distribution, and hence the buoyancy, in the system. Anhydrite precipitation thus will exert a negative feedback on the system that will modify both the rate of reduction in the porosity and permeability and their distribution within the recharge zone. The pertinent equations and boundary conditions, which are presented below, are solved numerically using finite differences. For simplicity, the shallow circulation shown in Figure 1 is neglected and the geometry of the model is shown in Figure 6. As in the constant flow case, the temperature at the top and bottom of the model are fixed at 0°C and 350°C , respectively.

[17] In the variable flow and heat transfer model, equation (1) remains unchanged. The heat transfer equation (3) now includes a time-dependent term and must be solved separately in the recharge and discharge zones. Thus,

$$\rho c \frac{\partial T}{\partial t} + c_f q \frac{\partial T}{\partial z} = \lambda \frac{\partial^2 T}{\partial z^2}, \quad (7)$$

where ρ and c represent the effective density and effective specific heat of the saturated porous medium, respectively. The mass flow rate q is given by Darcy's law:

$$q = -\frac{k}{\nu} \left(\frac{\partial P}{\partial z} - \rho_f g \right), \quad (8)$$

where k is the permeability of the porous medium, ν is the kinematic viscosity, and g is the gravitational acceleration. Equations (7) and (8) are coupled further through the equation of state, which relates the density of the fluid to its temperature:

$$\rho_f = \rho_{f0} (1 - \alpha_f T), \quad (9)$$

where $\rho_{f0} = 10^3 \text{ kg m}^{-3}$, corresponding to the density at the reference temperature $T = 0^\circ\text{C}$, and α_f is the coefficient of thermal expansion of water.

[18] We assume that the fluid is incompressible and employ the Boussinesq approximation, which states that variations in density only affect fluid buoyancy. We then rewrite Darcy's law by multiplying both sides of equation (8) by the cross-sectional area A through which the fluid flows, dividing both sides by the factor ν/kA , and integrating the resulting equation along the entire flow path L . That is,

$$Q \int_0^L \frac{\nu}{kA} dl = - \int_0^L \frac{\partial P}{\partial z} dl - \rho_{f0} \alpha_f g \int_0^L T(z) dl, \quad (10)$$

where the total mass flux $Q = qA$ is constant. The integral on the left of equation (10) is the total flow resistance R . The first term on the right-hand side of equation (10) vanishes upon integration around the whole flow path. The second term on the right of (10) is the total buoyancy head \hat{H} . Because T is a function of z , only this term can be written

$$\hat{H} = \rho_{f0} \alpha_f g \int_0^H [T_d(z) - T_r(z)] dz, \quad (11)$$

where the subscripts d and r refer to the discharge and recharge zones, respectively. Equation (10) can then be written

$$Q = \frac{\hat{H}}{R} = \frac{\rho_f \alpha_f g \int_0^H [T_d(z) - T_r(z)] dz}{\int_0^L \frac{\nu}{kA} dl}. \quad (12)$$

In this form, Darcy's law is equivalent to Ohm's law for electric currents [e.g., Elder, 1981; Lowell, 1991]. Hydrothermal models involving analogous forms of equation (12) have been used previously [e.g., Lowell, 1975, 1991; Pascoe and Cann, 1995; Germanovich et al., 2000, 2001].

[19] It is customary, however, to neglect the resistance in the horizontal section [e.g., Elder, 1981; Pascoe and Cann, 1995] and to consider only the resistance in the recharge and

discharge zones. This simplification is not critical to the results. We further assume areas of discharge and recharge zone do not change with time and depth. The total resistance in the recharge and discharge paths as a function of time t then becomes

$$R(t) = \frac{1}{A_r} \int_0^H \frac{\nu_r(z, t) dz}{k_r(z, t)} + \frac{1}{A_d} \int_0^H \frac{\nu_d(z, t) dz}{k_d(z, t)}. \quad (13)$$

To complete the equation set, an expression for $\nu(z, t)$ and a formula relating porosity and permeability are required. For viscosity we used an inverse temperature dependence as by *Germanovich et al.* [2000, 2001]:

$$\nu(z, t) = \frac{3.2 \cdot 10^{-5}}{15.4 + T(z, t)}. \quad (14)$$

Equation (14) for viscosity yields values of $2 \times 10^{-6} \text{ m}^2 \text{ s}^{-1}$ at $T = 0^\circ\text{C}$ to $9 \times 10^{-8} \text{ m}^2 \text{ s}^{-1}$ at $T = 350^\circ\text{C}$.

[20] To obtain the porosity-permeability relationship, we assumed a set of planar parallel cracks of width d and separation b . Then assuming $d \ll b$, $\phi \approx d/b$, and the relationship between permeability and porosity is [*Bear*, 1972]

$$k = \frac{b^2 \phi^3}{12}. \quad (15)$$

A cubic relationship between porosity and permeability is a rather general expression for porous and fractured media, so the results derived from using equation (15) are more general than might be thought [*Germanovich et al.*, 2001].

[21] We then solved the set of equations (2), (7), and (12) through (15) defining the full model using central finite differences in the spatial terms and explicit forward differencing in time. For given values of A_r and A_d , we started the model by assuming initial values of u (or equivalently Q), ϕ_0 , and k_0 . We then calculate the temperature distribution in both recharge and discharge zones by solving equation (7). With this temperature distribution, we calculate a new porosity and permeability in the recharge zone with equations (2) and (15), respectively. We then use equations (13), (14) and (15) in equation (12) to calculate a new flow rate Q . With these new values of Q , ϕ , and k we start the next iteration in time. At each time step we also calculate the heat output of the discharge zone. This is an observable parameter, and therefore it is a better descriptor of system behavior than mass flow rate. The total heat output $\hat{P}(t)$ is given by

$$\hat{P}(t) = c_f Q(t) T(t) + \lambda \frac{\partial T(t)}{\partial z} A_d. \quad (16)$$

Because we neglect lateral heat losses from the discharge zone, $\hat{P}(t)$ is constant everywhere within the discharge zone.

[22] To represent an initial high-temperature hydrothermal system, we used $\phi_0 = 0.01$ and $k_0 \approx 10^{-11} \text{ m}^2$. A value of $u = 10^{-7} \text{ m s}^{-1}$ was used to start the system. The purpose of these calculations was to explore how the feedbacks between anhydrite precipitation, permeability sealing, and hydrothermal heat output were affected by the size of the

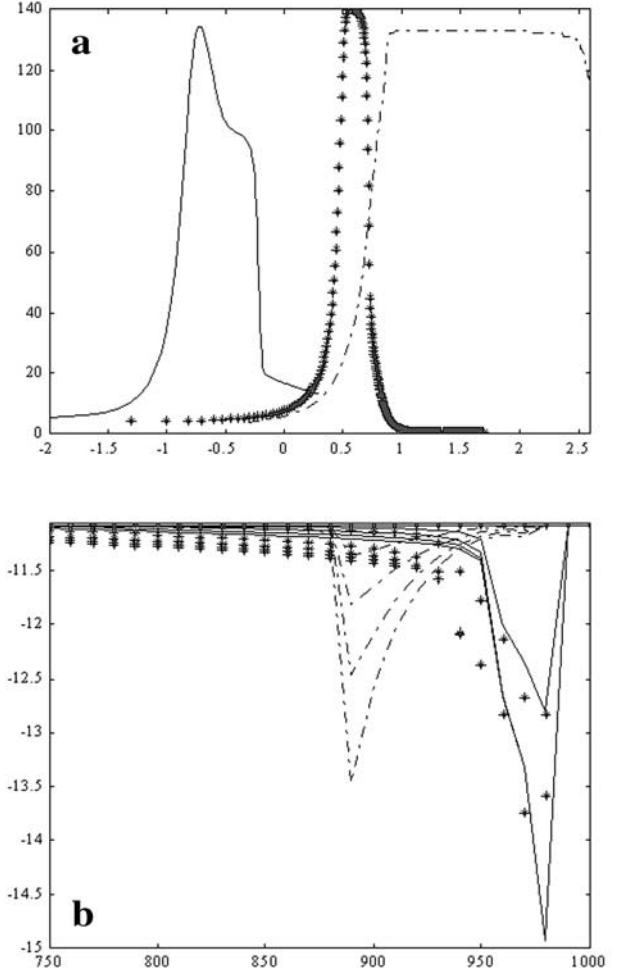


Figure 7. (a) Heat output (MW) of a single-pass hydrothermal system as a function of time for different ratios of recharge area to discharge area. Solid lines represent $A_r = A_d$; pluses represent $A_r = 10A_d$; dashed lines represent $A_r = 100A_d$. (b) Permeability contours as a function of depth as selected times. Solid lines represent contour intervals of 0.5 year; stars represent contour intervals of 20 years; and dashed lines represent contour intervals of 100 years, respectively. Symbols are same as for Figure 7a. For this case, $\phi_0 = 0.01$.

recharge area A_r . As a result, we considered cases in which $A_r = A_d$ and cases in which $A_r > A_d$.

[23] Figure 7a shows that when $A_r = A_d$, the heat output of the system decreases drastically within one year. Even if $A_r = 10A_d$, the heat output begins to decline within 10 years after reaching its peak. If $A_r = 100A_d$, however, a nearly constant flow rate, and hence heat output is maintained for more than 100 years. The reason for this is clear upon examination of the permeability as a function of time for the three cases. Figure 7b shows that when $A_r = A_d$, there is a rapid decrease in permeability of nearly 4 orders of magnitude concentrated near the base of the system. This large change in flow resistance inhibits flow and results in a rapidly declining heat output. As the area of the recharge zone increases, the rate of permeability decrease slows dramatically, and the decrease in permeability is spread

out over a greater depth interval. This effect also results in a decrease in the rate at which permeability is reduced. As a result, when $A_r = 100A_d$, the heat output remains nearly constant for hundreds of years.

4. Discussion

4.1. Robustness of the Model

[24] In the calculations performed above, anhydrite precipitation occurred between 150°C and 300°C as a consequence of the temperature dependence of anhydrite solubility in seawater. Because the concentration of SO_4^{2-} in seawater is ~ 3 times that of Ca^{2+} , the removal of Ca^{2+} in equal proportions with SO_4^{2-} to form anhydrite leaves a considerable amount of SO_4^{2-} in solution. Water-rock reaction experiments, however, show that Ca^{2+} begins to be released from basalt (in exchange for Mg^{2+} from seawater) when temperature exceeds 150°C [Bischoff and Dickson, 1975; Seyfried and Bischoff, 1981; Mottl, 1983]. The additional Ca^{2+} released from basalt may then combine with the remaining SO_4^{2-} in solution to precipitate more anhydrite. The amount of anhydrite precipitation calculated in this model is thus a lower estimate because we did not consider the additional anhydrite precipitation resulting from rock-water reaction. Moreover, we have also neglected the effect of other precipitates that may arise upon heating of seawater, such as magnesium oxysulfate [Bischoff and Seyfried, 1978] or that may result from low-temperature water-rock reactions. In spite of this underestimate, however, the calculations indicate that anhydrite will significantly reduce the permeability of the recharge zone and the heat output of the hydrothermal system in a short time unless the area of the recharge zone is much greater than that of the discharge zone. The fact that anhydrite precipitation in recharge zones does not appear to impact high-temperature hydrothermal circulation suggests therefore that the recharge areas are ~ 10 – 100 times larger than discharge areas. For this to be the case, recharge must occur from off axis and is likely to occur along axis as well.

[25] It is not essential, however, that recharge occur everywhere at once. It may be that recharge gets sealed in one area as a result of anhydrite precipitation and that another area of recharge becomes open, perhaps as a result of tectonic activity and fault activation, to replace it. As the initially sealed area cools and anhydrite dissolves, that area might again become accessible to recharge. As noted below, however, deeply deposited anhydrite is less likely to dissolve than that deposited higher in the crust. Because deeply deposited anhydrite is likely to occur over a relatively thin depth interval, it would be an effective barrier to flow for a considerable time.

[26] It is possible, however, either that anhydrite precipitation is not as significant as the model assumes or that the anhydrite does not simply clog the pore space at the site of precipitation. If anhydrite precipitation is not as significant as assumed, it could be because either Ca^{2+} or SO_4^{2-} is removed from seawater by other low-temperature processes. For example, Ca^{2+} could be removed in other low-temperature reactions (e.g., as CaCO_3) or SO_4^{2-} could be removed by sulfate-reducing bacteria in the subsurface. If anhydrite is not deposited in place as it is precipitated but is carried along by the fluid and is gradually deposited over some

distance, the overall flow resistance is lower than if the permeability is effectively sealed over a small depth interval. Finally, it may be that the assumption of thermodynamic equilibrium is faulty. If the kinetics of anhydrite precipitation is important, then the deposition of anhydrite could be spread out over a greater depth interval. In any of these circumstances, the effect of anhydrite precipitation on clogging permeable pathways would be reduced and hydrothermal output could be more easily maintained.

4.2. Model Implications

[27] The results in section 3 show that fluid flow rate (or permeability evolution) is an important factor in determining the distribution of anhydrite in the recharge zone of a seafloor hydrothermal system. There are some similarities between the constant flow and the full model. In both models, the greatest rate of porosity reduction occurs at a temperature of 150°C. In the constant flow rate model this isotherm occurs at greater depths as the flow rate increases. In the full single-pass model including the feedback of anhydrite precipitation on permeability, the depth of the 150°C isotherm is partly a function of recharge area. If the recharge area is small ($A_r \approx A_d$), the 150°C isotherm is initially near the base of the recharge zone and anhydrite is rapidly deposited in a thin layer. As the permeability becomes sealed and the flow rate slows, this isotherm becomes shallower. Thus there is a tendency for the region of anhydrite precipitation to spread with increasing time. The anhydrite initially precipitated at depth will remain in place provided the temperature at depth remains greater than 150°C. If $A_r \gg A_d$ as indicated by the model results, there is less tendency to deposit a thin layer of anhydrite deep in the system where it would be difficult to remove. In either case, as the crust moves off-axis and ages, the subsurface temperature will decline. Eventually, much of the anhydrite deposited during recharge will dissolve. Anhydrite deposited in thin layers near the base of the recharge zone would tend to be preferentially preserved and may be recycled to the mantle.

5. Conclusions

[28] The rate of anhydrite precipitation in hydrothermal recharge zones of ridge axis high-temperature seafloor hydrothermal systems is a strong function of recharge velocity, which in turn is a function of permeability and recharge area. The calculations in this paper show that anhydrite precipitation would rapidly seal hydrothermal recharge zones unless the recharge areas are 10–100 times larger than discharge areas. Recharge over large areas indicates that recharge occurs from off-axis as well as on-axis sites and is likely to be three-dimensional. Large recharge areas also suggest that the principal flow resistance in ridge crest hydrothermal systems stems from the discharge zones.

[29] **Acknowledgments.** The authors thank the reviewers, Norm Sleep and Jianwen Yang, and the Associate Editor, James Brennan, for their helpful comments on this manuscript. This work was supported by NSF grant OCE-9529954.

References

- Alt, J. C., J. Honnorez, C. Laverne, and R. Emmermann, Hydrothermal alteration of a 1 km section through the upper oceanic crust, deep sea drilling project hole 504B: Mineralogy, chemistry and evolution of seawater-basalt interactions, *J. Geophys. Res.*, 91, 10,309–10,335, 1986.

- Alt, J. C., T. F. Anderson, and L. Bonnell, The geochemistry of sulfur in a 1.3 km section of hydrothermally altered oceanic crust, DSDP hole 504B, *Geochim. Cosmochim. Acta*, 53, 1011–1023, 1989.
- Bear, J., *Dynamics of Fluids in Porous Media*, 764 pp., Elsevier Sci., New York, 1972.
- Becker, K., R. von Herzen, J. Kirklin, R. Evans, D. Kadko, M. Kinoshita, O. Matsubayashi, R. Mills, A. Schultz, and P. Rona, Conductive heat flow at the TAG active hydrothermal mound: Results from 1993–1995 submersible surveys, *Geophys. Res. Lett.*, 23, 3463–3466, 1996.
- Bischoff, J. L., and F. W. Dickson, Seawater basalt interaction at 200°C and 500 bars: Implications for the origin of seafloor heavy metal deposits and regulation of seawater chemistry, *Earth Planet. Sci. Lett.*, 25, 385–397, 1975.
- Bischoff, J. L., and W. E. Seyfried, Hydrothermal chemistry of seawater from 25° to 350°C, *Am. J. Sci.*, 278, 838–860, 1978.
- Blount, C. W., and F. W. Dickson, The solubility of anhydrite (CaSO₄) in NaCl-H₂O from 100° to 450°C and 1 to 1000 bars, *Geochim. Cosmochim. Acta*, 33, 227–245, 1969.
- Bowers, T. S., A. C. Campbell, A. Spivack, and J. Edmond, Chemical controls on the composition of vent fluids 13°–11°N and 21°N, East Pacific Rise, *J. Geophys. Res.*, 93, 4522–4536, 1988.
- Edmond, J. M., C. Measures, R. E. McDuff, L. H. Chan, R. Collier, B. Grant, L. I. Gordon, and J. B. Corliss, Ridge crest hydrothermal activity and the balances of the major and minor elements in the ocean: The Galapagos data, *Earth Planet. Sci. Lett.*, 46, 1–18, 1979.
- Elder, J. W., *Geothermal Systems*, 508 pp., Academic, San Diego, Calif., 1981.
- Elderfield, H., and A. Schultz, Mid-ocean ridge hydrothermal fluxes and the chemical composition of the ocean, *Annu. Rev. Earth Planet. Sci.*, 24, 191–234, 1996.
- Fontaine, F. J., M. Rabinowicz, and J. Boulègue, Permeability changes due to mineral diagenesis in fractured crust: Implications for hydrothermal circulation at mid-ocean ridges, *Earth Planet. Sci. Lett.*, 184, 407–425, 2001.
- Germanovich, L. N., R. P. Lowell, and D. K. Astakhov, Stress dependent permeability and the formation of seafloor event plumes, *J. Geophys. Res.*, 105, 8341–8354, 2000.
- Germanovich, L. N., R. P. Lowell, and D. K. Astakhov, Bifurcations in seafloor hydrothermal flow, *J. Geophys. Res.*, 106, 473–496, 2001.
- Haymon, R. M., D. J. Fornari, M. H. Edwards, S. Carbotte, D. Wright, and K. C. Macdonald, Hydrothermal vent distribution along the East Pacific Rise crest (9°09′–54′N) and its relationship to magmatic and tectonic processes on fast-spreading mid-ocean ridges, *Earth Planet. Sci. Lett.*, 104, 513–534, 1991.
- Jannasch, H. W., and C. O. Wirsen, Chemosynthetic primary production at East Pacific sea floor spreading centers, *BioScience*, 29, 592–598, 1979.
- Jannasch, H. W., Microbial processes at deep-sea hydrothermal vents, in *Hydrothermal Processes at Sea Floor Spreading Centers*, edited by P. A. Rona et al., pp. 677–709, Plenum, New York, 1983.
- Jannasch, H. W., Microbial interaction with hydrothermal fluids, in *Seafloor Hydrothermal Systems: Physical, Chemical, Biological, and Geological Interactions*, *Geophys. Monogr. Ser.*, vol. 91, edited by S. E. Humphris et al., pp. 273–296, AGU, Washington, D.C., 1995.
- Johnson, H. P., and M. Hutnak, Conductive heat loss in recent eruptions at mid-ocean ridges, *Geophys. Res. Lett.*, 24, 3089–3092, 1997.
- Lowell, R. P., Circulation in fractures, hot springs, and convective heat transport on mid-ocean ridge crests, *Geophys. J. R. Astron. Soc.*, 40, 351–365, 1975.
- Lowell, R. P., Modeling continental and submarine hydrothermal systems, *Rev. Geophys.*, 29, 457–476, 1991.
- Lowell, R. P., and D. K. Burnell, Mathematical modeling of conductive heat transfer from a freezing convecting magma chamber to a single-pass hydrothermal system: Implications for sea floor black smokers, *Earth Planet. Sci. Lett.*, 104, 59–69, 1991.
- Lowell, R. P., and L. N. Germanovich, On the temporal evolution of high-temperature hydrothermal systems at ocean ridge crests, *J. Geophys. Res.*, 99, 565–575, 1994.
- Lowell, R. P., and L. N. Germanovich, Evolution of a brine-saturated layer at the base of a ridge-crest hydrothermal system, *J. Geophys. Res.*, 102, 10,245–10,255, 1997.
- Lowell, R. P., P. V. Cappellen, and L. N. Germanovich, Silica precipitation in fractures and the evolution of permeability in hydrothermal upflow zones, *Science*, 260, 192–194, 1993.
- Martin, J. T., and R. P. Lowell, Precipitation of quartz during high-temperature, fracture-controlled hydrothermal upflow at ocean ridges: Equilibrium versus linear kinetics, *J. Geophys. Res.*, 105, 869–882, 2000.
- McDuff, R. E., and J. M. Edmond, On the fate of sulfate during hydrothermal circulation at mid-ocean ridges, *Earth Planet. Sci. Lett.*, 57, 117–132, 1982.
- Mottl, M. J., Metabasalts, axial hot springs, and the structure of hydrothermal systems at mid-ocean ridges, *Geol. Soc. Am. Bull.*, 94, 161–180, 1983.
- Mottl, M. J., H. D. Holland, and R. F. Corr, Chemical exchange during hydrothermal alteration of basalt by seawater, II, Experimental results for Fe, Mn and sulfur species, *Geochim. Cosmochim. Acta*, 43, 869–884, 1979.
- Pascoe, A. R., and J. R. Cann, Modeling diffuse hydrothermal flow in black smoker vent fields, Hydrothermal vents and processes, in *Hydrothermal Vents and Processes*, 87, edited by L. M. Parson, C. L. Walker, and D. R. Dixon, *Geol. Soc. Spec. Pub.*, 159–173, 1995.
- Phillips, O. M., *Flow and Reactions in Permeable Rocks*, 277 pp., Cambridge Univ. Press, New York, 1991.
- Sclater, J. G., C. Jaupart, and D. Galson, The heat flow through oceanic and continental crust and the heat loss of the Earth, *Rev. Geophys.*, 18, 269–311, 1980.
- Seyfried, W. E., Jr., and J. L. Bischoff, Experimental seawater-basalt interaction at 300°C, 500 bars, chemical exchange, secondary mineral formation and implication for the transport of heavy metals, *Geochim. Cosmochim. Acta*, 45, 135–147, 1981.
- Shank, T. M., D. J. Fornari, K. L. von Damm, M. D. Lilly, R. M. Haymon, and R. A. Lutz, Temporal and spatial patterns of biological community development at nascent deep-sea hydrothermal vents along the East Pacific Rise, *Deep Sea Res., Part II*, 45, 465–515, 1998.
- Shanks, W. C., J. L. Bischoff, and R. J. Rosenbauer, Seawater sulfate reduction and sulfur isotope fraction in basaltic systems: interaction of seawater with fayalite and magnetite at 200–350°C, *Geochim. Cosmochim. Acta*, 45, 1977–1995, 1981.
- Sleep, N. H., Hydrothermal circulation, anhydrite precipitation and thermal structure at ridge axes, *J. Geophys. Res.*, 96, 2375–2387, 1991.
- Stein, C. A., and S. Stein, Constraints on hydrothermal heat flux through the oceanic lithosphere from global heat flow, *J. Geophys. Res.*, 99, 3081–3095, 1994.
- Teagle, D. A. H., J. C. Alt, and A. N. Halliday, Tracing the chemical evolution of fluids during hydrothermal recharge: Constraints from anhydrite recovered in ODP Hole 504B, *Earth Planet. Sci. Lett.*, 155, 167–182, 1998.
- Thompson, G., Basalt-seawater interaction, in *Hydrothermal Processes at Seafloor Spreading Centers*, *NATO Conf. Ser. IV*, vol. 12, edited by P. A. Rona et al., pp. 225–278, Plenum, New York, 1983.
- Von Damm, K. L., Controls on the chemistry and temporal variability of seafloor hydrothermal fluids, in *Seafloor Hydrothermal Systems: Physical, Chemical, Biological, and Geological Interactions*, *Geophys. Monogr. Ser.*, vol. 91, edited by S. E. Humphris et al., pp. 222–247, AGU, Washington, D.C., 1995.
- Von Damm, K. L., J. M. Edmond, B. Grant, C. I. Measures, B. Walden, and R. Weiss, Chemistry of submarine hydrothermal solutions at 21°N, East Pacific Rise, *Geochim. Cosmochim. Acta*, 49, 2107–2220, 1985.
- Williams, D. L., and R. P. von Herzen, Heat loss from the Earth: New estimate, *Geology*, 2, 327–328, 1974.
- Wolery, T. J., and N. H. Sleep, Hydrothermal circulation and geochemical flux at mid-ocean ridges, *J. Geol.*, 84, 249–275, 1976.
- Wood, J. R., and T. A. Hewett, Fluid convection and mass transfer in porous sandstones—a theoretical model, *Geochim. Cosmochim. Acta*, 46, 1707–1713, 1982.
- Yao, Y., Anhydrite precipitation and evolution of permeability in ocean ridge crest hydrothermal systems, M.S. thesis, 81 pp., Ga. Inst. of Technol., Atlanta, 2001.

R. P. Lowell and Y. Yao, School of Earth and Atmospheric Sciences, Georgia Institute of Technology, 221 Bobby Dodd Way, Atlanta, GA 30332-0340, USA. (bob.Lowell@eas.gatech.edu)